Chemical Engineering Science 298 (2024) 120383

Contents lists available at ScienceDirect

Chemical Engineering Science

journal homepage: www.elsevier.com/locate/ces

Polystyrene-reduced graphene oxide composite as sorbent for oil removal from an Oil-Water mixture

Isaiah Olufemi Akanji [a,b], Samuel Ayodele Iwarere [c,*], Badruddeen Saulawa Sani [d], Bello Mukhtar [a], Baba El-Yakubu Jibril [a,**], Michael Olawale Daramola [c]

[a] Department of Chemical Engineering, Ahmadu Bello University, Zaria, Nigeria
[b] National Oil Spill Detection and Response Agency (NOSDRA), Ilorin Zonal Office, Ilorin, Nigeria
[c] Department of Chemical Engineering, Faculty of Engineering, Built Environment and Information Technology, University of Pretoria, Hatfield 0028, Pretoria, South Africa
[d] Department of Water Resources and Environmental Engineering, Ahmadu Bello University, Zaria, Nigeria

ARTICLE INFO

Keywords:
Adsorbent
Graphene
Composite
Electrospinning
Adsorption

ABSTRACT

This study enhanced the adsorptive capacity of polystyrene (PS) by infusing reduced graphene oxide (rGO) nanoparticles obtained from the synthesis of graphene oxide to produce PS-rGO composites via electrospinning method. Physicochemical characterization of as-synthesized rGO and PS-rGO were carried out through scanning electron microscopy, N_2 physisorption among others. Oil sorption performance of synthesized rGO in crude oil, vegetable oil, fresh engine oil and used engine oil are 130.96 g/g, 121.77 g/g, 105.01 g/g and 100.56 g/g. Oil sorption capacities of electrospun pure PS in crude oil, vegetable oil, fresh engine oil and used engine oil were 46.32 g/g, 38.54 g/g, 35.14 g/g and 32.57 g/g and those of PS-rGO infused with 4 wt% of rGO were found to be 105.52 g/g, 98.86 g/g, 86.25 g/g and 83.47 g/g for crude oil, vegetable oil, fresh engine oil and used engine oil samples respectively. Pseudo second order (PSO) kinetic model fits the sorption data of the four oil samples on the four composite sorbents produced. Intra-particle diffusion (IPD) model evidently showed that sorption of the four oil samples on the four composite sorbents, occurred in three (3) phases. Composites demonstrate high oil adsorption capacity, and are reusable upto three sorption–desorption cycles.

1. Introduction

Leakages of over 800 tons of lubricants, diesel and heavy oils into the ocean by MV Wakashio vessel off the coast of Mauritius in July 2020 and similar spillages have occurred frequently around the world, Davide et al. (2021). Among oil spill cleanup methods, adsorption is commonly used due to its simplicity, low capital and operational cost, as well as high removal efficiency, Elanchezhiyan et al. (2018). Organic sorbents like polypropylene (PP) and polyurethane (PU) sponges, that are synthetic in nature and available commercially are porous and known to have characteristics such as low cost, excellent buoyancy, large-scale availability, high oleophilic and hydrophobic characteristic, Saleem et al. (2015). Natural organic as well as natural inorganic sorbents like wool, zeolites and activated carbon are microporous, and are known to have limitations such as poor adsorption capacities, poor selectivity for oil adsorption and difficult reusability, Noor and Tatjána, (2016). Therefore, cleaning of oil spills has been associated with enormous solid waste generation. The International Tanker Owners Pollution Federation Limited (ITOPF) reported in (2018) that, volume of waste generated after oil spill clean-up can be as much as ten times volume of oil originally spilt. Their work proposed the use of reusable oil sorbents as a potential alternative, ITOPF (2018). However, development of these sorbents are still at infancy. Recently, Wu et al. (2017) elucidate the use of nanotechnology involving application of electrospinning machine for the fabrication of nanostructure materials like nanofibers which have features such as high selectivity for oil relative to water, high porosity and specific surface area. In electrospinning, application of electrostatic force helps to drag a thin jet of conductive solution, for the production of continuous micro and nanofibers which have controllable structure and composition. Consequently, a new type of adsorbent which has significant advantages and improved properties over conventional oil adsorbents emerged, Li et al. (2014).

* Corresponding author. Tel: +27 12 420 3902.
** Co-corresponding author.
E-mail addresses: samuel.iwarere@up.ac.za (S.A. Iwarere), byjibril@gmail.com (B.E.-Y. Jibril).

https://doi.org/10.1016/j.ces.2024.120383
Received 13 November 2023; Received in revised form 12 June 2024; Accepted 13 June 2024
Available online 15 June 2024

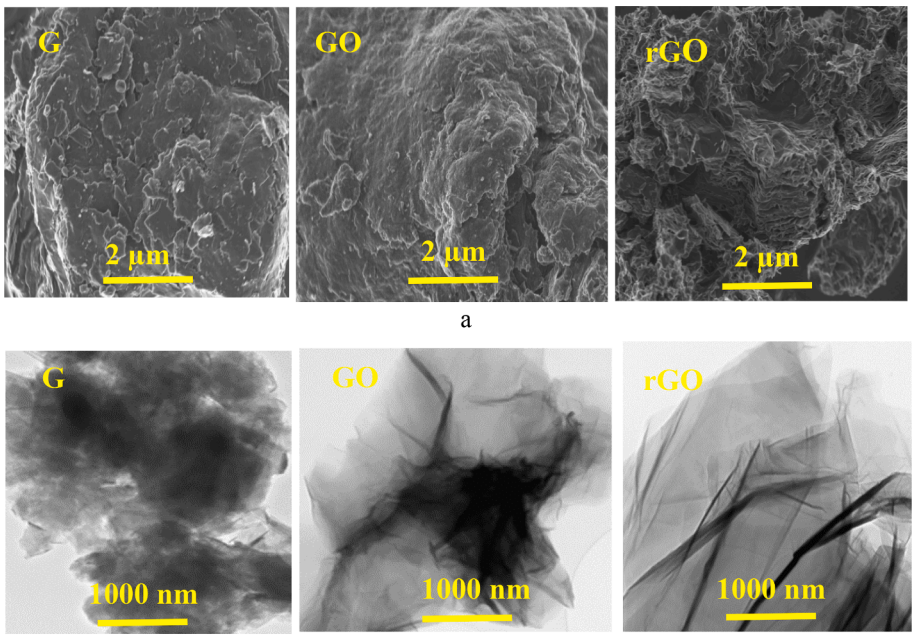

Fig. 1. (a). Graphite, Graphene Oxide and reduced Graphene Oxide Morphologies (b): – TEM images of Graphite, Graphene Oxide and reduced Graphene Oxide.

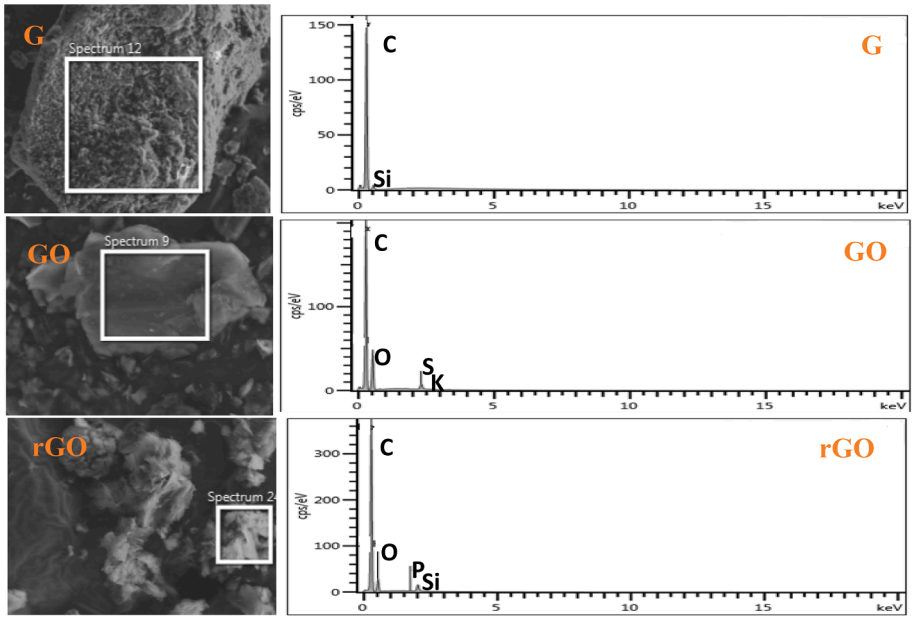

Fig. 2. EDX Spectra of Graphite, Graphene Oxide and reduced Graphene.

Sorption capacities of most PS-based fibers are approximately four times higher than that of natural organic adsorbents and non-woven polypropylene (PP) fiber mattresses as recently demonstrated by, Lakayan et al. (2020). However, PS sorbents exhibit mechanical properties that are poor, which therefore render them susceptible to being damaged when transported or treated after oil spills clean-up, and unsuitable for reuse Wu et al. (2017). Materials such as iron oxide (Fe_3O_4), polyacrylonitrile (PAN), polyvinylidene fluoride (PVDF) had been introduced as fillers to modify their mechanical strength, but Jiang et al. (2015) reported that incorporation of such fillers decreased the surface area, as well as sorption capacities of resulting sorbents.

Earlier studies by Gupta and Tai (2016) revealed that oil–water separation potential of carbon nanotubes (CNTs) is excellent, owning to their low density, extremely high specific surface area, oleophilic-hydrophobic nature. Report of Wu et al. (2017) therefore leveraged on the unique properties of CNTs, and used it as a nanofiller in electrospun polystyrene nanofibers, called PS-CNTs composite sorbent. The PS-CNTs composite fibers produced by the authors displayed high sorption capacity of 111.45–122.88 g/g when used to adsorb motor, sunflower and peanut oils, in comparison to when ordinary electrospun PS sorbents which displayed sorption capacity of 70.90–83.19 g/g was applied. Modified properties of their composites such as smaller diameters of fiber and higher specific surface area was responsible for the improved sorption capacity.

Boccaccini, (1997) further reported that extensive research works showed that electrical conductivity of composite materials depends largely on their microstructures. Lakayan et al. (2020), corroborated that, electrical conductivity of electrospun PS solution increased by the

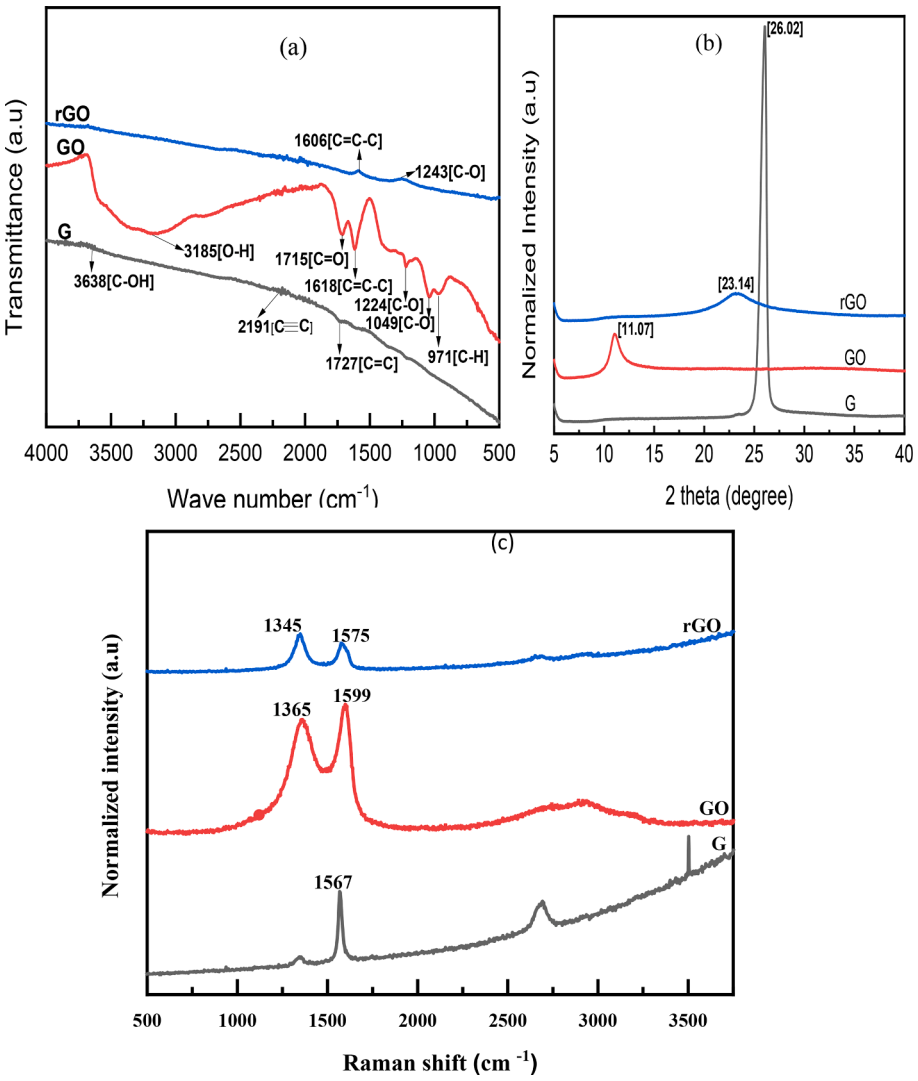

Fig. 3. a: FTIR spectral of Graphite, Graphene Oxide and reduced Graphene Oxide b: – XRD patterns of Graphite, Graphene Oxide and reduced Graphene Oxide c: – Raman Spectra of Graphite, Graphene Oxide and reduced Graphene Oxide.

addition of nanoclay such as Cloisite 20A, which in turn increased the elasticity of fiber and its rapidity to stretch towards the collector drum of an electrospinning machine, to produce fibers with narrower diameter.

Nanoparticles such as Cloisite 20A and CNTs used as fillers in PS composite have electrical conductivity 200 μS/cm and (1000 S/cm–100,000 S/cm) respectively, at room temperature (Timo, 1998; Parmoor et al., 2020) and their specific surface area have been reported to be 750 m^2/g and 1315 m^2/g respectively (Al-Marri et al., 2017; Peigney et al., 2001). However, single layer graphene possesses higher electrical conductivity, approximately 6000 S/cm, as well as, larger theoretical surface area, about 2630 m^2/g, Becerril et al. (2008), where chirality is not a factor limiting its conductivity, Sandeep et al. (2017), when compared to Cloisite 20A and CNT.

Previous studies had infused Cloisite 20A, CNTs and other nanoparticles in commercially available PS, to produce electrospun PS-nanocomposites sorbents with narrow diameter fibers. These nanoparticles, had been reported to have physical properties such as electrical conductivity and specific surface area, relatively lower than those of rGO. In the present study, the material used as nanofiller in waste PS solution has superior electrical conductivity and specific surface area. Higher electrical conductivity of rGO aids production of highly charged electrospun solution, and the speed with which droplets of polymer solution jets towards the collector drum during electrospinning, hence producing composite with much narrower fiber diameters and significantly larger surface area. This is the novelty of this research work.

The main contribution of this paper therefore is in twofold; the first is to investigate how infusion of rGO with a higher electrical conductivity create a highly charged electrospun polymer solution, when commercially available PS is replaced by waste PS plastic, and ultimately produce composite fibers with narrower diameters. Secondly is to exploit the high specific surface area of rGO to produce composite fibers with improved surface area and oil sorption capacity.

2. Experimental section

2.1. Materials

Sodium Nitrate (99 %), Potassium permanganate (99 %), Sulphuric Acid (98 %), Hydrogen Peroxide (30 %) and Hydrochloric acid (37 %) were procured by Glassworld and Chemical Suppliers, South Africa. Natural Graphite (50μ), Iodine resublimed, N, N-Dimethylformamide and Hypophosphorous Acid (50 wt% in H_2O) were supplied by Sigma-Aldrich, South Africa. Polystyrene (plastic waste) was collected from an electronic store in Oyo, Nigeria. Motor and vegetable oils were, purchased from a gas station and shopping mall in Lagos Nigeria, respectively. Used engine oil was collected from an automobile

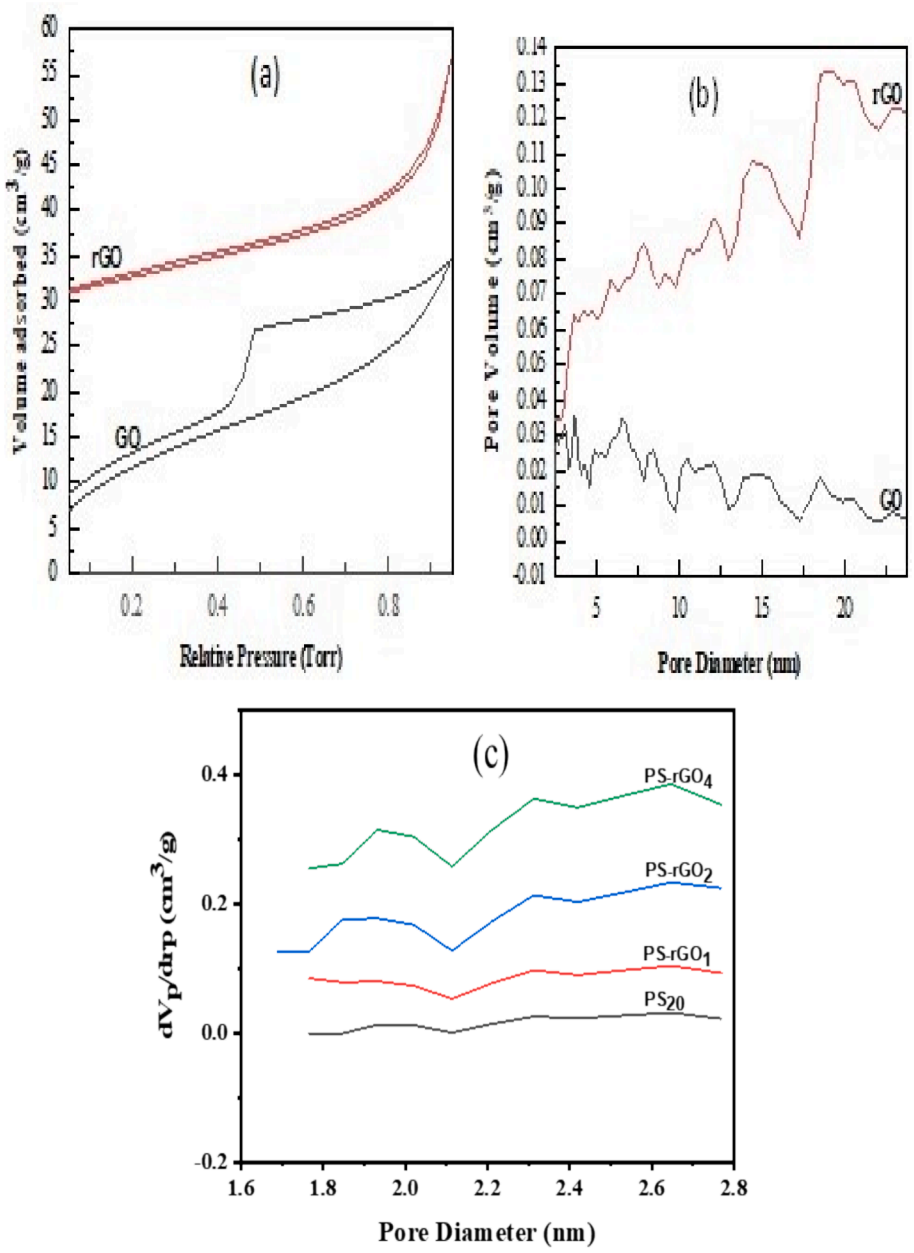

Fig. 4. (a). Nitrogen adsorption–desorption isotherms of GO and rGO (b). DFT pore distribution curves of GO and rGO (c). Pore size distribution of PS and PS-rGO Composites.

Table 1
Pore size, pore volume and specific surface areas of graphite (G), graphene oxide (GO) and reduced graphene oxide (rGO).

Samples	Average Pore Size (nm)	Total Pore Volume (cm^3/g)	BET Surface Area (m^2/g)
G	8.252	0.013	16.608
GO	7.625	0.032	81.083
rGO	6.365	0.047	140.570

Table 2
Pore sizes, pore volumes and surface areas of composites.

S/No	Composites	DR Pore diameter (nm)	DR Pore Volume (cm^3/g)	BET Surface Area (m^2/g)
1	PS_{20}	6.435	0.02519	71.50
2	PS-rGO_1	3.866	0.06990	137.881
3	PS-rGO_2	5.740	0.08509	208.745
4	PS-rGO_4	6.366	0.10410	285.072

workshop in Lagos, Nigeria. Deionized water was used.

2.2. Graphene Oxide (GO) preparation

Graphene Oxide was synthesized by the modified form of the method developed by Hummer and Offeman (1957). A 1000 mL beaker was placed in a chilling system (WiseCircu; UNIV VAN PTA; 758540) which was mounted with an overhead stirrer (Celsius; UNIV VAN PTA; 949542). Exactly 130 mL of concentrated H_2SO_4 was accurately measured into the beaker, and 5 g of natural graphite (50 μm) was weighed and poured into it under stirring at 0 °C. After stirring for about 5 min, 2.5 g of $NaNO_3$ was introduced and, stirring continued for additional 2 h. 15 g of $KMnO_4$ was added and the temperature was kept

(c). Pore size distribution of PS and PS-rGO Composites

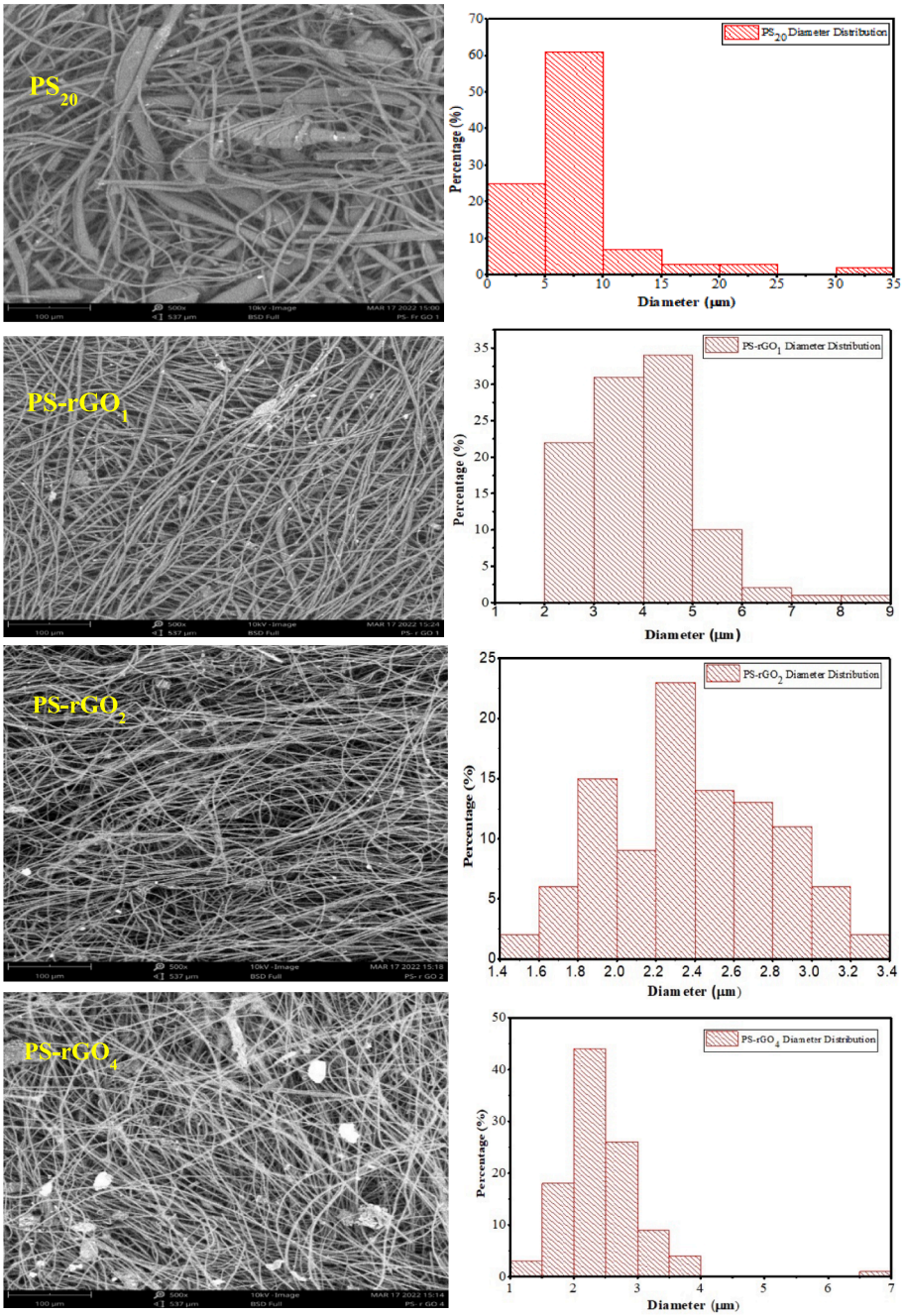

Fig. 5. Morphology of electrospun PS infused with rGO and Fiber Diameter Distribution 5b: –SEM Images Showing Blank PS (PS_{20}) and Interaction of PS and rGO ($PS\text{-}rGO_4$).

at 10 °C, the mixture was further stirred for 2 h. Temperature was monitored to ensure it does not exceed 20 °C, thereafter, it was raised to 35 °C in an ultrasonic cleaner (Model PS-80) with stirring for 30 min and the temperature was monitored. Exactly, 230 mL deionized water was added drop-wise and slowly, this resulted to an exothermic reaction which raised the temperature of the suspension to about 98 °C. The temperature was then maintained at 98 °C in a heating bath (BUCHI Heating Bath; Type B-491; SN 1000212040) for about 30 min under continuous stirring. The suspension was allowed to cool in air and then placed in cold bath for 30 min, before adding another 500 mL deionized water under continuously stirring. Resulting mixture was later treated with about 5 mL H_2O_2 (30 %), which was followed by continuous stirring for 10 min, in the cold bath. There was a colour change from dark brown to brilliant yellow, which indicates formation of Graphene Oxide (GO). The mixture was allowed to settle overnight under gravity, the water layer was carefully decanted. The GO solution was then washed three times with 1 M dilute HCl, under centrifuge (Hettich ZENTRIFUGEN; ROTOFIX 46H) at 2000 rpm, to remove metal ions. Finally, the GO solution was thoroughly washed in deionized water under vacuum filtration until its pH became neutral. Yellow brown filter cake of

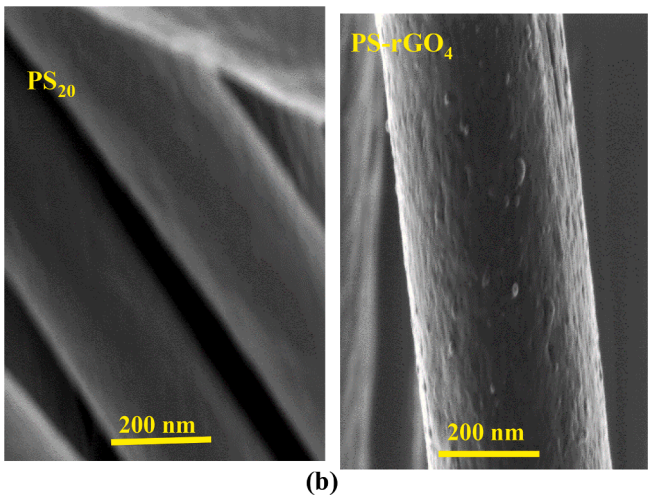

Fig. 5. (*continued*).

Table 3
Fiber diameter of electrospun composites sorbents from their SEM images.

S/NO	Composites	Fiber Diameters (μm)
1	PS_{20}	3.84672
2	PS-rGO_1	5.72231
3	PS-rGO_2	2.37690
4	PS-rGO_4	2.32860

GO was then obtained, and dried in air.

2.3. Reduced Graphene Oxide (rGO) synthesis

Graphene Oxide modifications to rGO was achieved through chemical reduction method, Jin-Yong et al. (2015). GO powder (90 mg) was carefully dispersed in 22.5 mL deionized water (4 mg/mL), thereafter 7.5 mL of Hypophosphorous Acid (H_3PO_2) was accurately measured and mixed with the aqueous GO solution. About 900 mg of iodine (I_2, 99.5 %, Aldrich) was introduced to the suspension, such that; GO: H_3PO_2:I_2 was 1:100:10. The suspension was sonicated in an Ultrasonic Cleaner (Model PS-80) for 5 min at 30 °C, and was transferred into an oven (LABEX: FMH instruments; SHK-IN) where it was heated for 8 h at 80 °C. After the heating, a black gel was formed. The rGO wet gel formed was removed from the oven, and cooled down to room temperature in a fume cupboard. rGO produced was finally washed in ethanol and deionized water (ratio 1:1) until its pH became neutral. Finally, it was freeze-dried for 72 h.

Table 4
Physical properties of oil samples used for adsorption test.

S/No	Oil Samples	Viscosity (mPa.S)	Density (g/cm^3)
1	Crude Oil	50.17	0.8347
2	Vegetable Oil	133.10	0.8482
3	Fresh Engine Oil	242.20	0.8728
4	Used Engine Oil	386.55	0.8893

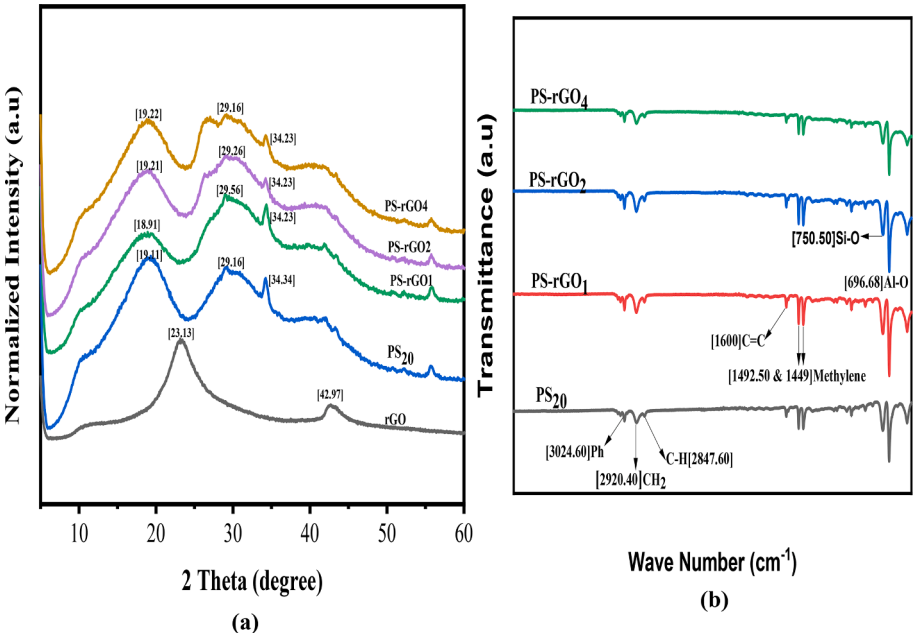

Fig. 6. a: XRD Patterns of rGO, PS and PS-rGOs Composite Sorbents b: – FTIR Spectra of PS and PS-rGO composite sorbents.

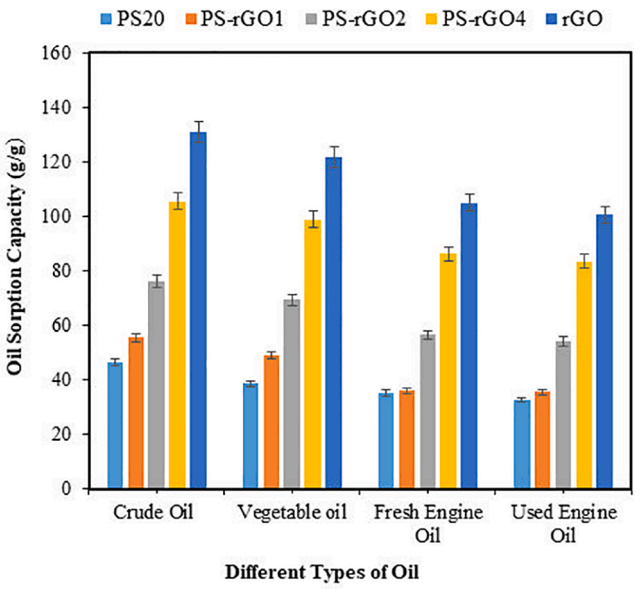

Fig. 7. Maximum oil sorption capacities of different sorbents.

Table 5
R^2 and SSE (%) values of three kinetic models for the sorption of four oil samples.

Oil Samples	Kinetic Models	R^2	SSE (%)
Crude Oil	PFO	0.9059–0.9887	1.2850–3.0120
	PSO	0.9847–0.9872	6.9706–9.0054
	IPD;		
	R_1^2	0.9332–0.9537	–
	R_2^2	0.9667–0.9956	–
Vegetable Oil	PFO	0.9565–0.8461	1.9852–9.8838
	PSO	0.9921–0.9989	0.5817–1.6062
	IPD;		
	R_1^2	0.9404–0.9684	–
	R_2^2	0.9062–0.9486	–
Fresh Engine Oil	PFO	0.8080–0.9835	1.1442–5.6206
	PSO	0.9938–0.9986	0.7233–1.4977
	IPD;		
	R_1^2	0.9419–0.9672	–
	R_2^2	0.8405–0.9498	–
Used Engine Oil	PFO	0.8620–0.9677	0.4291–0.6663
	PSO	0.9851–0.9960	0.47844–0.77174
	IPD;		
	R_1^2	0.8905–0.9848	–
	R_2^2	0.3134–0.9423	–

2.4. Formation of PS-rGO composites by electrospinning

In a 250 mL beaker, 20 wt% polystyrene (PS) was dissolved using N, N-Dimethylformamide (DMF). The PS-solution was stirred on a magnetic stirrer (DATHAN MNH-20D) set at 250 rpm for one hour. Three separate concentrations (1, 2 and 4 wt%) of rGOs was later mixed with the dissolved PS solution. They were labelled PS-rGO_1, PS-rGO_2, and PS-rGO_4, respectively. To obtain homogenous mixtures, the composites were further stirred on the magnetic stirrer at 250 rpm for another 1 h, and subsequently sonicated at 30 °C in an ultrasonic cleaner (Celsius Scientific-Model PS-80) for 30 min. IME Technology Electrospinning Platform (V4 HMI engine MKI) used in fabricating the PS and PS-rGO composite, consists of the following; DC high-voltage supplier, a syringe pump, and a rotating collector drum. About 10 mL of PS-rGOs was sucked into a 15 mL capacity syringe, and was clamped, and the syringe pump was set at 0.5 mL/hr. Rotating drum collector was lined with aluminum foil and set at 100 rpm, with a high voltage set at 15 KV. Needle used was 0.8 mm in diameter, and 15 cm needle to collector distance was maintained. Electrospinning was done at 28 °C and 64 % relative humidity. Finally, electrospun composite sheets were removed carefully from the collector, placed in an oven set at 60 °C and allowed to stay overnight, to evaporate residual solvent.

2.5. Characterization of rGO and PS-rGOs composite sorbents

The microstructures of graphite (G), GO, rGO, PS and PS-rGOs was obtained from a field emission scanning electron microscope, FE-SEM, (Zeiss Ultra Plus 55) model which has an energy dispersive X-ray (EDX) operated at 2.0 kV, attached. Fiber diameter of electrospun composites were obtained from their morphological images by using Image J. G, GO, rGO, PS and PS-rGOs Fourier transform-infrared (FTIR) analysis was carried out using Varian FT-IR spectroscopy at (500–4000 cm^{-1}) wavenumber range. Transmission electron microscopy analysis (TEM) of G, GO, rGO was achieved using a very high-resolution transmission electron microscope, JEOL-2100F, (HRTEM FEI Tecnai-F30) alongside 200 kV acceleration voltage operated at 1.0 kV.

A Benchtop X-ray diffraction (XRD) analyzer (Bruker BV 2D PHASER Best) with reflection geometry at 2θ values (5–900) and a step size of 0.0050, operating with a Cu Kα1 radiation source (λ = 0.15406 nm) at 50 kV and 30 mA was employed to analyze the Phase structure of G, GO, rGO, PS and PS-rGOs. The samples were further characterized with WITec alpha 300 RAS + Confocal micro-Raman microscope. In order to avoid heating the samples, it was operated at 532 nm laser wavelength, spectral acquisition time of 150 s and laser power of 5 mW. Surface area of G, GO and rGO were measured by N_2 adsorption at 77.35 K (BET) using a St 1 on NOVA touch 2LX [S/N: 1050003126] instrument, after degassing for 3 h at 373 K. Those of PS-rGOs were determined by N_2 adsorption at 273 K (BET) using quantachrome instruments, after degassing for 1 h at 373 K.

2.6. Sorption studies

For each of PS, PS-rGOs electrospun composite nanofibers, maximum oil sorption capacity was obtained in pure oil, using three different oil samples in a batch adsorption. In the adsorption test, 100 mL of used engine oil was accurately measured into a clean 250 mL beaker and 0.15 g of PS_{20} was carefully cut out of the electrospun fibers, and accurately weighed on a weighing balance (DM.3 Digital Scale). It was then immersed in used engine oil for 60 min. Upon saturation, the oil ladened sorbent was retrieved with a tweezer, allowed to drained for 10 s, mass of sorbent with oil was taken and maximum oil sorption (Q_{max}) evaluated. This was repeated for two other oil samples, motor oil and vegetable oil, with PS_{20} and other PS-rGOs. Equation (1) was employed to calculate oil adsorption capacity, Pourjavadi et al. (2013).

$$Q = M_1 - M_0/M_0 \quad (1)$$

where;

Q = Oil uptake capacity of sorbents (g/g); M_0 = Dry mass of adsorbent before adsorption test (g) and M_1 = Wet mass of adsorbent after adsorption (g). All experiments were performed at room temperature, data were obtained in triplicate, to ensure repeatability of results.

2.7. Oil sorption kinetics

Oil sorption kinetics are used to establish the relationship between concentration of adsorbate in solution and the rates of oil uptake. It is further used to derive information on time needed to attain equilibrium, mechanism controlling adsorption process, as well as adsorbent-adsorbate interaction pathways. In this research work, three kinetics models were used to study the kinetics of four different oil samples on

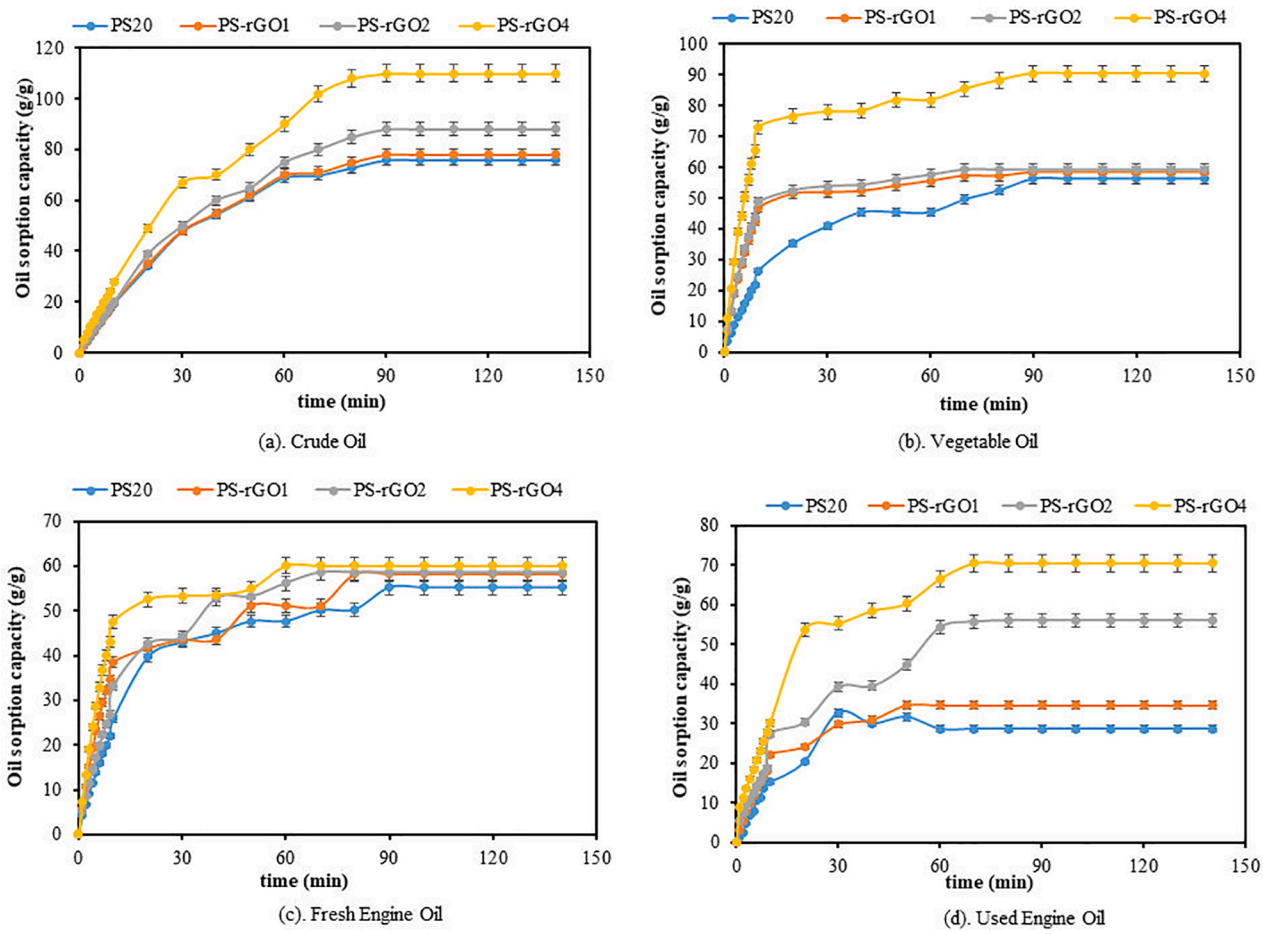

Fig. 8. Sorption kinetics of four different sorbents (PS_{20}, PS-rGO_1, PS-rGO_2 and PS-rGO_4) in four different types of oils.

the produced composites oil sorbents, PS-rGOs. The models include Pseudo-first-order (PFO), Pseudo-second-order (PSO) and Intraparticle diffusion (IPD) models.

Equation (2) described Pseudo first-order kinetic model; Lakayan et al. (2020)

$$\frac{dq_t}{dt} = k_1(q_1 - q_t) \tag{2}$$

$$ln(q_e - q_t) = lnq_e - k_1 t \tag{3}$$

Where; q_t represents adsorbate amount adsorbed at any time t, g/g; q_e stand for amount of adsorbate adsorbed at equilibrium, g/g; and k_1 is Pseudo-first order rate constant, in 1/min.

Pseudo second-order model, based on the equilibrium adsorption capacity is described by Eq. (4); Ahmad et al. (2005); Lakayan et al. (2020).

$$\frac{dq_t}{dt} = k_2(q_e - q_t)^2 \tag{4}$$

$$\frac{t}{q_t} = \frac{1}{K_2 q_e^2} + \frac{t}{q_e} \tag{5}$$

q_t stand for the amount of adsorbate adsorbed at any time t, g/g; while q_e is the amount of adsorbate adsorbed at equilibrium, g/g; and k_2 is Pseudo-second order rate constant, in g/g min.

Intraparticle diffusion (IPD) model was utilized to describe the oil sorption mechanism, with IPD model, one adsorption can be divided into multiple linear equations, as shown in Eq. (6); Ahmad et al. (2005); Lakayan et al. (2020).

$$q_t = k_{dif} t^{1/2} + C \tag{6}$$

q_t is the amount of oil adsorbed at time t, g/g; and k_{dif} is the intraparticle diffusion rate constant, in $g/gmin^{0.5}$. C is a constant, which is the intercept of the straight line graph, and related to the boundary layer thickness (g/g).

Based on the experimental data obtained from sorption of the four oil samples, straight line equations were fitted and regression coefficients, (R^2) value were obtained, and fitness of each of the models were investigated.

2.8. Regeneration and reusability evaluation

For the regeneration of produced adsorbents, and to investigate the reusability of PS-rGO_1, PS-rGO_2 and PS-rGO_4, after the sorption process, the oil ladened sorbents were compressed between two flat plates, to desorb the oil. They were then rinsed in ethanol and in deionized water, and subsequently placed in an oven maintained at 60 °C until dryness. After drying, the regenerated composite sheets were reused until a structural collapse was observed.

3. Results and discussion

3.1. Morphological structures of G, GO and rGO

Surface morphology of the synthesized samples is shown in Fig. 1a. The graphite (G) shows a rocky morphology with no obvious porous structure. GO is characterized by layered structure, with ultrathin and homogeneous graphene films, which are folded and shows

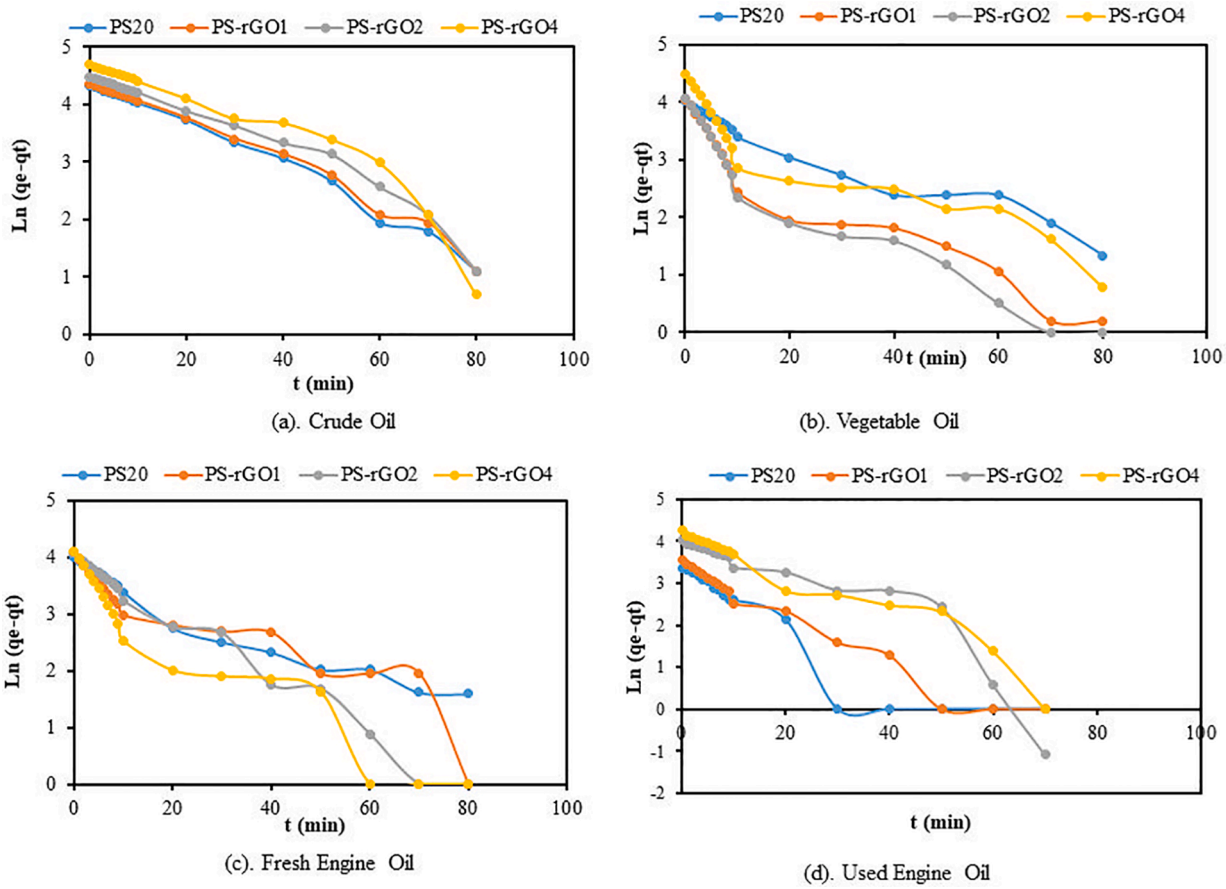

Fig. 9. Sorption of four oil samples with PS_{20}, PS-rGO_1, PS-rGO_2 and PS-rGO_4 based on Pseudo First Order (PFO) kinetics.

distinguishing edges of individual sheets, as well as wrinkled areas. This agrees with the observation of, Leila et al. (2014). Upon chemical reduction of GO to rGO, dispersibility of graphene sheets in an aqueous system was lost, graphene sheets so produced was found flexible, and then coalesced and overlapped on each other, thereby forming a well-defined, porous and 3D framework. This agrees with the observation of Pin-Hsuan et al. (2017).

Similarly, G, GO and rGO TEM images are presented in Fig. 1b. Sheet like nature of graphene oxide nanomaterials and changes in morphology associated with reduction were confirmed by obtaining Transmission electron microscopy (TEM) images. In the TEM image of graphite (G), a tight aggregate within the host sheets is shown, with the formation of bulk nanostructure, with no distinctive sheet and exhibition of lower interlayer spacing. In the TEM image of GO, thinner flaky, wrinkles and folds were formed from dispersed aggregated sheets. Strong interconnection between building blocks of GO was depicted in the 3D network. This is consistent with the report of, Pin-Hsuan et al. (2017). Reduction of GO to rGO is accompanied by development of more folds. More wrinkles, twists and folds are observed at the edges of graphene sheets in rGO as compared to GO. When viewed under microscope, rGO exhibits internal cellular structure, with pores that are interconnected. Due to reduction process; the pore walls changed into assembled graphene sheets. This shows that graphene sheets produced a 3D porous structure by cross-linking, and then assembled to form larger sheets. This is consistent with the observation of, Ren et al. (2017).

3.2. EDX of G, GO and rGO

Fig. 2 depicts the EDX Spectra of natural graphite (G), graphene oxide (GO) and reduced Graphene Oxide (rGO). Natural graphite (G) primarily composed of carbon with a trace of silicon, Graphene Oxide (GO) and reduced Graphene Oxide (rGO) are essentially carbon and oxygen with traces of minor elements such as Potassium, Sulphur, Silicon and Phosphorous. About 22.72 % oxygen available on Graphene Oxide suggests successful oxidation of graphite to graphene oxide (GO). Similarly, a decrease in the percentage composition of oxygen, to 12.50 % after treatment of GO with Hypophosphorous Acid and Iodine suggests its successful reduction to rGO. This result agrees with the report of, Delvina et al. (2020).

3.3. FTIR Spectra of G, GO and rGO

Natural Graphite (G), Graphene Oxide (GO) and reduced Graphene Oxide (rGO) FTIR analysis are displayed in Fig. 3a. Spectrum of G shows faint peaks around 3638 cm^{-1}, 2191 cm^{-1} and 1727 cm^{-1} which are correspond to the nonbonded hydroxyl (–OH) group stretch, triple bonds (C≡C) stretch and characteristic vibrations of unsaturated (C=C) double bond. Reports of Faniyi et al. (2019), agree with this result. Similarly, spectrum of GO shows typical peaks appearing at 3185 cm^{-1}, 1715 cm^{-1}, 1618 cm^{-1}, 1224 cm^{-1}, 1049 cm^{-1} and 971 cm^{-1} which are, respectively, assigned to O-H stretch, Carbonyl (C=O) stretching, aromatic ring (C=C-C), ring, epoxy (C-O) bond, alkoxy (C-O) bond and trans (C-H) hydrogen group. Spectrum of rGO shows that peaks at 3185 cm^{-1} and 1715 cm^{-1} are conspicuously absent, and that at 1224 cm^{-1} was found to be weakened in intensity and broadened. This implies some Oxygen-Containing functional groups were removed as GO was reduced to rGO. This is consistent with the report of, Oribayo et al. (2017).

3.4. G, GO and rGO XRD patterns

XRD according to matching card no. JCPDS N96-120-0018 was adopted to investigate the phase-structure of as-synthesized samples.

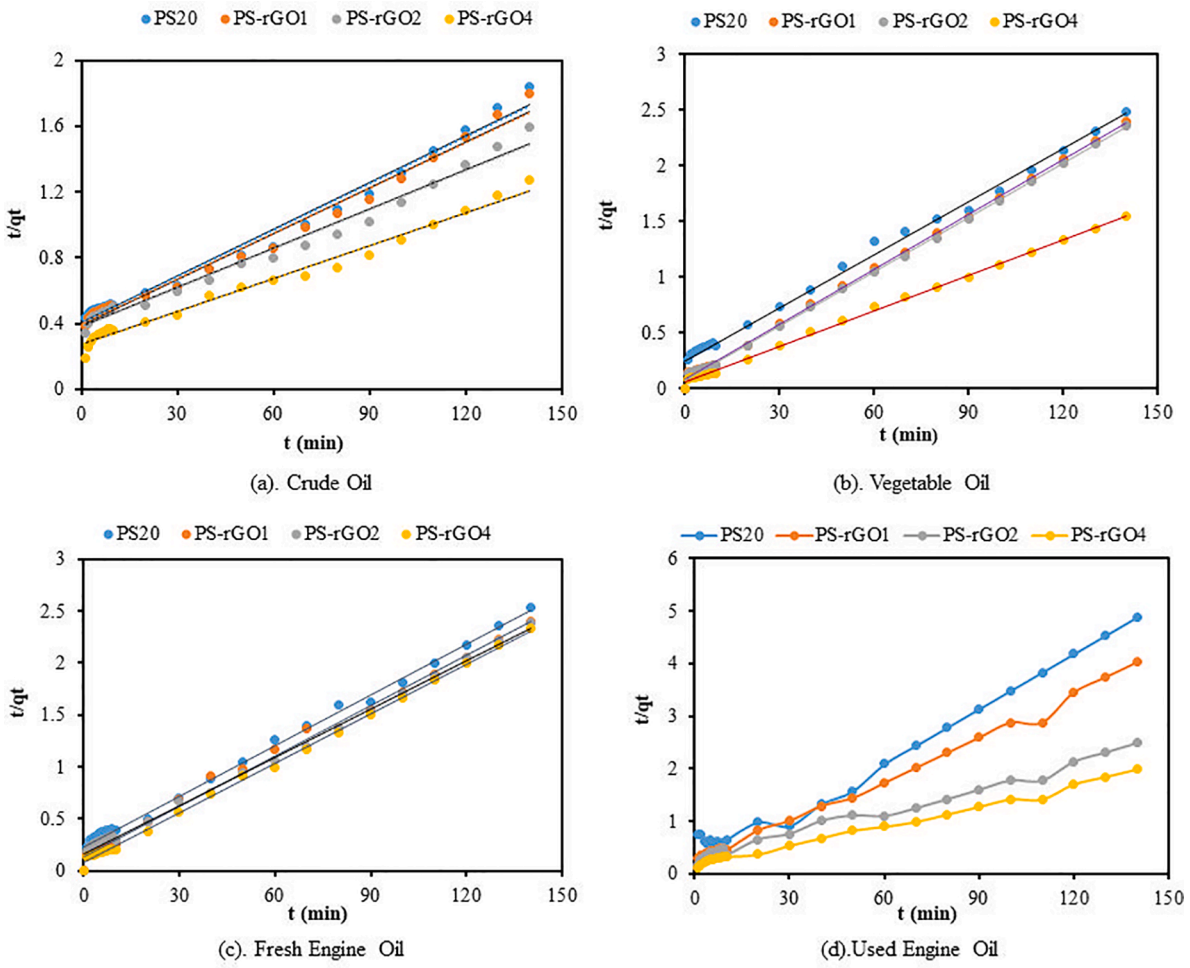

Fig. 10. Sorption kinetics of four different oil samples with ps_{20}, PS-rGO_1, PS-rGO_2 and PS-rGO_4 based on Pseudo second order (PSO) kinetics.

Fig. 3b shows the XRD patterns of pristine graphite (G), Graphene Oxide (GO) and reduced Graphene Oxide (rGO), measured within angular range $2\theta = 5^0$–40^0. In the XRD patterns, narrow diffraction peak of G at $2\theta = 26.02^0$ corresponds to interlayer spacing of 3.35 Å. Upon oxidation of G to GO, the peak a new diffraction peak appeared at $2\theta = 11.07^0$, corresponding to interlayer spacing 7.97 Å. This shows by interlayer spacing, carbon structure increased instantaneously with oxidation of graphite Wang et al. (2012). A new diffraction peak, faint and much broadened appeared at $2\theta = 23.14^0$ and interlayer spacing of 3.82 Å, after the reduction of GO to rGO, this suggests patterns similar to that of an amorphous carbon structure in rGO synthesized. The interlayer spacing of rGO (3.82 Å) is close to that of G (3.35 Å). When compared to G, rGO migrates to a lower 2θ, which indicates a change of interlayer spacing, suggesting that interlayer spacing of rGO layers is much larger in rGO than in G. Therefore, these shows that GO to rGO occurred successfully during the chemical reduction step, Pin-Hsuan et al. (2017).

3.5. Raman Spectra of G, GO and rGO

In order to understand the molecular structures of G, GO and rGO samples Raman Spectroscopy measurement was used. Raman spectra of the samples are presented in Fig. 3c. In the spectrum of graphite, a broad G-band is shown at 1567 cm^{-1} and faint D-band at 1353 cm^{-1} corresponding to disordered graphitic lattice. Density of defects in the carbon material was established using peak intensity ratio of D-peak to G-peak (I_D/I_G). I_D/I_G of Graphite (G) is 0.20 showing that G is in its undisturbed graphitic form. For GO, G-band appeared around 1599 cm^{-1} and D-band around 1365 cm^{-1} which depicts a disordered graphitic lattice, with I_D/I_G of GO is 0.94. Existence of D-band and G-band of rGO at 1341 cm^{-1} and 1579 cm^{-1}, respectively, near standard location at 1350 cm^{-1} and 1580 cm^{-1} confirms that graphene is present in rGO. Its ratio of I_D/I_G is 1.05 shows that the produced graphene is highly defective.

3.6. Specific surface area

3.6.1. Specific surface area of GO and rGO by BET

Fig. 4a and Fig. 4b, show the adsorption–desorption isotherm and pore distribution curves obtained with method based on density functional theory (DFT), for both Graphene Oxide (GO) and reduced Graphene Oxide (rGO), respectively. From Fig. 4a, Type IV adsorption–desorption isotherm and Type H3 hysteresis loop, corresponding to existence of mesopores could be observed, for rGO. From DFT pore size distribution curves of GO and rGO in Fig. 4b, pore diameter of GO and rGO was 7.625 nm and 6.365 nm, respectively, indicating that both GO and rGO have porosity in the mesoporous range. Similarly, activated carbon produced by Alvarez-Torrellas et al. (2023), for removal of antibiotics, using refinery sludge and urban wastewater treatment plant sludge, activated by KOH and $ZnCl_2$ (R-KOH, U-KOH, R-$ZnCl_2$ and U-$ZnCl_2$) equally show average pore sizes in the range (2.57–4.31) nm which are mesopores. The pore volume of GO and rGO were 0.0317 cm^3/g and 0.0466 cm^3/g, respectively. The BET surface area of GO and rGO were 81.084 m^2/g and 140.571 m^2/g, respectively. These BET values are relatively low, compared with those of activated carbon, (183 m^2/g–603 m^2/g) produced by Alvarez-Torrellas et al. (2023). However, significant increase in values after reduction implies that chemical reduction of GO to rGO enhanced the surface area of rGO

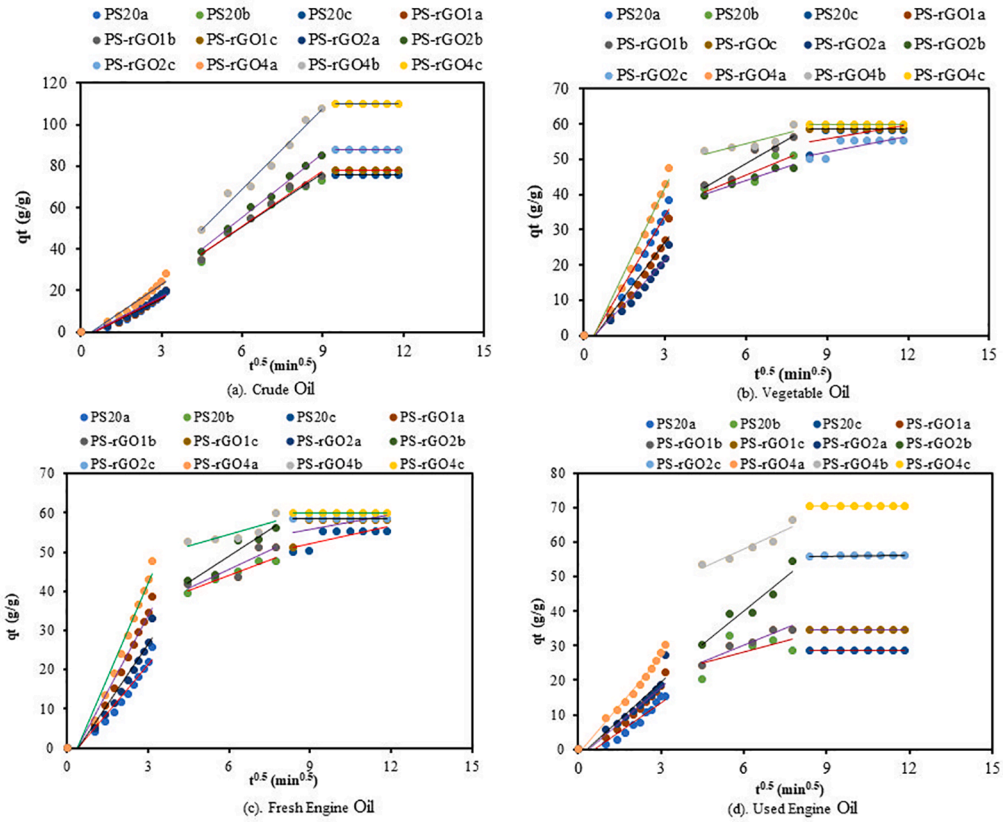

Fig. 11. Adsorption of four different types of oils with PS_{20}, PS-rGO_1, PS-rGO_2 and PS-rGO_4, based on Intraparticle Diffusion (IPD) model kinetics.

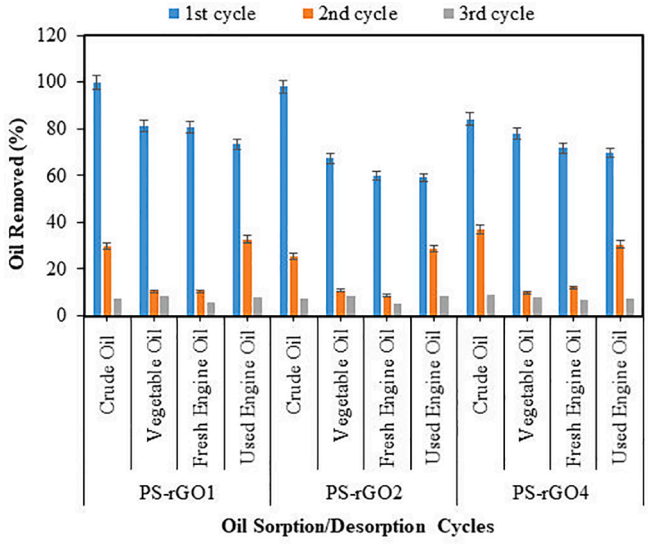

Fig. 12. Variation of Oil removal efficiency of composite sorbents with sorption cycles.

significantly, due to formation of assembled and porous structures. These results are summarized in Table 1.

3.6.2. *BET surface area of PS and PS-rGOs composite sorbents*

Fig. 4c presents the DFT pore size distribution of PS and PS-rGOs. From the pore size distribution, it is evident that pore diameter of PS and PS-rGOs is greater than 2 nm. As clearly presented in Table 2, pore volume obtained by DR-plot (micropore volume) method as well as BET surface areas of all the composites increased as weight ratio of rGO in the polystyrene increased. The BET surface area of PS-rGO_1 is almost twice that of PS_{20}; that of PS-rGO_2 is about three times the surface area of PS_{20}; and those of PS-rGO_4 is about four times greater than the surface area of PS_{20}. Clay-based adsorbents produced by Pablo et al. (2024) for removal of ciprofloxacin shows BET surface area in the range of (9.90–50.10) $m^2 g^{-1}$, which is far lower than those of pure PS and PS composite with rGO produced in this research, however the total pore volumes of the two sets of sorbent are within the same range. With this result, it is confirmed that infusion of rGO, with large surface area, into waste polystyrene solution enhanced significantly the surface area and pore volume of (PS-rGOs) composites. With rGO in PS waste plastic composites produced show significantly larger surface area than those with CNTs and Cloisite 20A reported by (Wu et al., 2017; Lakayan et al., 2020).

3.7. *Morphology of electrospun PS and PS-rGOs sorbents*

Earlier works on electrospun polystyrene have established 20 wt% of PS in DMF as yielding desirable adsorption property as well as stable fiber upon electrospinning. PS solution was separately infused with three different rGO concentrations i.e. (1, 2, and 4 wt%) to produce PS-rGO composite sorbent. Fig. 5a presents the morphology of PS and PS-rGOs composites sorbents, and Fig. 5b shows the interaction of rGO particles attached to the surface of the PS after electrospinning. The observed morphology and fiber diameter size of electrospun sorbents mainly depend on dispersibility of rGO in polymer solution, as well as, electrical conductivity of resulting PS-rGO solution. Infusion of rGO increases the electrical conductivity of PS_{20} solution which in-turn increases the elasticity and tendency of the fiber to stretch towards the rotating collector and ultimately decreased the fiber diameter size, Boccaccini (1997). Smaller diameter sized electrospun fibers with high porosity yield larger specific surface area. Average fiber diameter of PS-rGO_2 and PS-rGO_4 are lower than those of PS_{20}. This finding indicates that, notwithstanding the increase in the electrical conductivity of PS

solution by the addition of rGO in PS-rGO$_1$, the filler might not be well dispersed in the PS/DMF system. This eventually, resulted in aggregation of rGO and consequently larger fiber diameters. Composites (PS-Cloisite 20A) obtained by, Lakayan et al. (2020) showed narrower fibers compared to composites obtained in this study, this could be due to similar reason. This result is further summarized in Table 3.

3.8. XRD patterns of rGO, electrospun PS and PS-rGOs sorbents

XRD patterns of rGO, PS$_{20}$ and PS-rGO$_1$, PS-rGO$_2$ and PS-rGO$_4$ are presented in Fig. 6a. As earlier stated, rGO shows pattern of amorphous carbon structures with diffraction peaks at 23.13° and 42.97°. PS$_{20}$ shows diffraction peaks at 19.11°, 29.16° and 34.34°, but when rGOs (1, 2, 4 wt%) were infused into PS there were no new peaks formed. Obviously, PS and PS-rGOs essentially show similar XRD patterns, which implies that when rGO was dispersed in the polymer matrix, it lost part of its parallel and regular layered structure, which suggests that rGO agglomerates completely in the polymer matrix.

3.9. FTIR Spectra of PS and PS-rGOs composites

Fig. 6b presents the FTIR of PS and PS-rGO composite sorbents. Spectra of PS-rGOs have similar bends as those of PS$_{20}$, three distinct peak regions are common to all composites. Adsorption peak regions at 3024.60 cm^{-1} corresponds to the phenyl group (Ph). Those around 2920.40 and 2847.60 cm^{-1} are assigned to stretching vibration of CH_2 and C-H respectively. In the second region, peaks at 1600 cm^{-1}, 1492.50 cm^{-1} and 1449 cm^{-1} respectively correspond to the olefinic conjugated C=C bond as well as bending vibration of methylene. In the third peak region, 750.50 cm^{-1} signifies Si-O, and 696.68 cm^{-1} correspond to the stretching vibration of Al-O. Peak Locations representing certain functional groups in PS$_{20}$ are found to be almost the same as it is in PS-rGOs. This suggests that infusion of rGO in the polymer matrix does not affect the segmented structure of the polystyrene. However, infusion of rGO into PS$_{20}$ is observed as to contribute significantly to the hydrophobic nature of resultant electrospun composite fibers. Therefore, this confirms that there are no chemical interactions between rGOs and PS$_{20}$, as rGO is a mere nanofiller. This is not at variance with the report of, Lakayan et al. (2020).

3.10. Performance evaluation

3.10.1. Performance of PS and PS-rGOs as oil sorbents

The four fabricated electrospun composite sorbents (PS$_{20}$, PS-rGO$_1$, PS-rGO$_2$ and PS-rGO$_4$) were investigated for oil sorption as well as sorption contributions of rGO, in four pure oil media. Viscosity of oil samples has been known to have either caused an increase or a decrease in the oil uptake. It could causes an increase in adsorption because of oil adhesion to the fiber surface, or a decrease in adsorption when the oil is prevented from penetrating into the fiber interior area. As summarized in Table 4, viscosity of oil samples used in this study follows the following order of magnitude. Used Engine Oil > Fresh Engine Oil > Vegetable Oil > Crude Oil. The Oil sorption potential of PS and PS-rGOs composite sorbents in cleaning up oil spill was investigated. As produced sorbents were immersed in pure oil medium, because oil sorption mechanism is different when effects of water were considered. Maximum sorption capacity of different sorbents in four oils are presented in Fig. 7.

In the four oils samples considered, PS-rGO$_4$ shows the highest oil sorption capacity. Its modified properties, improved specific area and low fiber diameter, could be responsible. Oil sorption capacities of composites, in the three oil samples, increased as the quantity of rGO in the PS-matrix increased. PS$_{20}$ showed the lowest oil sorption capacity. PS-rGO$_1$ has low sorption capacity compared to PS-rGO$_4$, partly due to its large electrospun fiber diameter. PS-rGO$_4$ attained oil sorption capacity in the range of (83.47–105.52) g/g, a value two times larger than oil sorption capacity of commercially available synthetic polypropylene oil sorbents reported by, Aboul-Gheit et al. (2006) and about six times higher than sorption capacity of synthetic polypropylene in crude oil, reported by, Oribayo et al. (2017).

3.10.2. Kinetics of oil sorption with PS and PS-rGOs oil sorbents

Three adsorption kinetics models were used to study the rate and mechanism of sorption of four oil samples using PS and PS-rGOs composite sorbents produced in this research. These models includes pseudo-first-order model (PFO), pseudo-second-order model (PSO) and intra-particle diffusion (IPD) models. How best these models fits the oil sorption data was estimated by the coefficient of linear regression, R square (R^2) values as well as percentage Sum of Error Squares (SSE, %) which were computed and presented in Tables 5. The closer the R^2 to unity, and the lower the SSE, the better the fitness of the models to the experimental data.

Simulated oily water used in this experiment was prepared by mixing 10 g each of the four oil samples with 150 mL distilled water. A predetermined mass of the electrospun PS-rGOs composite sorbents was floated on the oily-water mixtures surface. As shown in Fig. 8a, sorption of Crude Oil on PS and PS-rGOs increased rapidly within the first 30 min, it slows down significantly in the next 50 min and attained equilibrium between (80–100) min. Also for Vegetable Oil, Fresh Engine Oil and Used Engine Oil sorption with the produced composites, sorption increases rapidly within the first 20 min, slows down in the next 30–60 min and attained equilibrium within 70–90 min, this is presented in Fig. 8b–d.

Kinetics of sorption of four different oil samples based on pseudo-first-order (PFO) and pseudo-second-order kinetic models (PSO), using the produced composites are presented in Fig. 9(a–d) and Fig. 10(a–d). In the sorption of four oil samples considered, Pseudo-second-order kinetics fits the experimental data better with R^2 values closest to unity, this agrees with the results of Wu et al. (2017) and Lakayan et al. (2020). The R^2 data is presented in Tables 5. Sorption of the four oil samples, based on the intraparticle diffusion (IPD) model, using the produced composites is shown in Fig. 11(a–d). IPD model clearly reveal that sorption of the four oils samples with the four sorbents is divided into three (3) different Phases. At different loading of rGO (0, 1, 2 and 4 wt%) on the waste polystyrene, IPD plots did not pass through the origin, hence producing a non-zero inter intercepts. For the adsorbate-adsorbent interaction, the non-zero intercept suggests that, oil sorption rate is affected by multiple parameters. These parameters include density, viscosity, surface area, porosity, surface tension as well as oleophilicity, this agrees with the results obtained by Mookgo et al. (2020). In the first and second oil sorption phases, the coefficient of linear regression, R^2 values based on IPD model, shows a good fit with experimental data, in the four cases studied.

3.10.3. Adsorption-desorption cycles and reusability of PS and PS-rGOs

Enormous waste generation and environmental impacts is attached to oil spill cleanups. Consequently, reusability of oil sorbents is a serious factor to consider in a bid for waste minimization, after oil spill cleanup. Previous reports have shown PS$_{20}$ as having weak mechanical strength, Wu et al. (2017) therefore its reusability after oil sorption was not tested. However, after infusion of rGO in PS, reusability of PS-rGO composites were then tested. PS-rGO$_1$ and PS-rGO$_2$ as well as PS-rGO$_4$ remained effective, after three successive sorption/desorption cycles. From Fig. 12, it is evident that, after the first sorption cycle, the three composites, showed an appreciably high oil recovery rates in crude oil, 29.85 %, 25.49 % and 36.96 % for PS-rGO$_1$, PS-rGO$_2$ and PS-rGO$_4$ respectively. A sharp drop in oil removal rates was observed, for all composite, after the second oil sorption cycle, in the four oil samples. These results indicate the effectiveness and reusability of PS-rGOs after three sorption–desorption cycles. Low number of sorption cycle could be attributed to the inability of cross-linked graphene nanosheets to influence appreciable mechanical properties of microstructures in the

resultant composite, as well as, accumulation of residual oils that remained entrained in the pores of the sponges, which cannot be removed by manual squeezing.

4. Conclusions

rGO which possess large specific surface areas, 140.57 m^2/g and high hydrophobicity was successfully synthesized. It shows high effectiveness for oil sorption. Sorption capacities of the rGO in crude oil, vegetable oil, fresh engine oil and used engine oils are 130.96 g/g, 121.77 g/g, 105.01 g/g and 100.56 g/g respectively. Due to aggregation, PS and PS-rGO composites obtained in the present study exhibits larger fiber diameters than those of PS-Cloisite 20A reported by, Lakayan et al. (2020). rGO infused in waste PS plastic was found to produce composites with significantly larger surface area than those infused with CNTs and Cloisite 20A reported by (Wu et al., 2017; Lakayan et al., 2020). Infusion of rGO in PS enhanced the surface area of the PS-rGO composites and in-turn led to a proportionate increase in their oil sorption capacities. BET surface area of pure PS is 71.52 m^2/g that of PS-rGO_4 is this 285.07 m^2/g. Similarly, sorption capacities of PS-rGOs improved significantly with rGO loading. Sorption capacity of pure PS in crude oil is 46.32 g/g, and that of PS-rGO_4 is 105.52 g/g. Surface area and sorption capacities, of produced composites are larger than those reported by Wu et al. (2017) and Lakayan et al. (2020). Based on the R^2 value, PSO kinetic model fits the sorption data of the four oil samples on the four composite sorbents produced. As evident from IPD model, Sorption of the four oil samples on the four composite sorbents, occurred in three (3) phases. Multiple parameters affect the sorption rate of all oil samples considered on the four composite. Few of them include oil viscosity, density, Surface Area, Surface Tension, Porosity, oleophilicity. PS-rGO composites are effective after three sorption–desorption cycles which offers them significant potential for reusability.

Funding

This research work was supported by Petroleum Technology Development Fund, (PTDF) (PTDF/ED/LSS/PHD/AOI/0368/19), Abuja, as well as PTDF Chair in Chemical Engineering of Ahmadu Bello University, Zaria, Nigeria.

CRediT authorship contribution statement

Isaiah Olufemi Akanji: Conceptualization, Formal analysis, Funding acquisition, Investigation, Methodology, Writing – original draft. **Samuel Ayodele Iwarere:** Project administration, Supervision, Writing – review & editing, Resources. **Badruddeen Saulawa Sani:** Supervision, Visualization, Writing – review & editing. **Bello Mukhtar:** Visualization, Writing – review & editing. **Baba El-Yakubu Jibril:** . **Michael Olawale Daramola:** Funding acquisition, Project administration, Supervision, Writing – review & editing, Resources.

Declaration of competing interest

The authors declare that they have no known competing financial interests or personal relationships that could have appeared to influence the work reported in this paper.

Data availability

The data collected have been analysed and included in the manuscript

Acknowledgement

We acknowledge the supports of Nanomaterial Industrial Development Facility, of DST-CSIR Nanotechnology Innovation Centre, of the Department of Science and Technology, Pretoria, Republic of South Africa.

References

Aboul-Gheit, A.K., Khalil, F.H., Abdel-Moghny, T., 2006. Adsorption of spilled oil from seawater by waste plastic. J. Oil Gas Sci. Technol. 259–268. https://doi.org/10.2516/ogst:2006019x.

Ahmad, A.L., Sumathi, S., Hameed, B.H., 2005. Adsorption of residue oil from palm oil mill effluent using powder and flake chitosan: Equilibrium and kinetic studies. Water Res. 39, 2483–2494.

Al-Marri, M.J., Masoud, M.S., Nassar, A.M.G., Zagho, M.M., Khader, M.M., 2017. Synthesis and Characterization of Poly (vinyl alcohol); Cloisite 20A Nanocomposite. J. Vinyl Addit. Tech. 181–187 https://doi.org/10.1002/vnl.21496.

Alvarez-Torrellas, S., Segura, Y., de Mora, A., Gutierrez-Śanchez, P., Sanz-Santos, E., Corrochano, N., Larriba, Pariente, M.I., Martínez, F., García, J. 2023. Evaluation of the adsorptive and catalytic properties of sludge-based carbon materials for the efficient removal of antibiotics listed in the European Decision 2020/1161/EU, *J. Environ. Chem. Eng.* ***11*** (1), 110–743. 10.1016/j.jece.2023.110743.

Becerril, H.A., Mao, J., Liu, Z., Stoltenberg, R.M., Bao, Z., Chen, Y., 2008. Evaluation of solution processed reduced graphene oxide films as transparent conductors. ACS Nano 2, 463–470. https://doi.org/10.1021/nn700375n.

Boccaccini, A.R., 1997. Predicting the electrical conductivity of two-phase composite materials. Script. Mater. 36 (10), 1195–1200. https://doi.org/10.1016/S1359-6462(97)00017-1.

Davide, S., Yohan, D.L., Simone, M., Paolo, G., Francesco, S., 2021. The Mauritius oil spill: what's next. MDPI J./Pollutants 1, 18–28. https://doi.org/10.3390/pollutants1010003.

Delvina, J.T., Oyedotun, K.O., Mirghni, A.A., Manyala, N., 2020. Sulphur-reduced graphene oxide composite with improved electrochemical performance for supercapacitor applications. Int. J. Hydrogen Energy 45, 13189–13201. https://doi.org/10.1016/j.ijhydene.2020.03.059.

Elanchezhiyan, S.S.D., Prabhu, S.M., Meenakshi, S., 2018. Effective adsorption of oil droplets from oil-in-water emulsion using metal ions encapsulated biopolymers: Role of metal ions and their mechanism in oil removal. Int. J. Bio. Macromol. 112 (2018), 294–305. https://doi.org/10.1016/j.ijbiomac.2018.01.118.

Faniyi I. O., Fasakin O., Olofinjana B., Adekunle A. S., Oluwasusi T. V, Eleruja M. A, Ajayi E. O. B., 2019. The comparative analyses of reduced graphene oxide (RGO) prepared via green, mild and chemical approaches, *Springer Nat. J., Applied Sci.,* 1–1181. 10.1007/s42452-019-1188-7.

Gupta, S., Tai, N.H., 2016. Carbon materials as oil sorbents: a review on the synthesis and performance. J. Mater. Chem. A4, 1550–1565. https://doi.org/10.1039/C5TA08321D.

Hummer, W.S., Offeman, R.E., 1957. Preparation of graphitic oxide. J. Am. Chem. Soc. 80, 1339. https://doi.org/10.1021/ja01539a017.

ITOPF. 2018. The International Tanker Owners Pollution Federation Limited (ITOPF); Technical Information Paper on Disposal of Oil and Debris. Retrieved May 24, 2018, from .

Jiang, Z., Tijing, L.D., Amarjargal, A., Park, C.H., An, K.-J., Shon, H.K., Kim, C.S., 2015. Removal of oil from water using magnetic bicomponent composite nanofibers fabricated by electrospinning. Compos. Part B Eng. 77, 311–318. https://doi.org/10.1016/j.compositesb.2015.03.067.

Jin-Yong, H., Sohn, E.-H., Park, S., Park, H.S., 2015. Highly-efficient and recyclable oil absorbing performance of functionalized graphene aerogel. Chem. Eng. J. 269, 229–235. https://doi.org/10.1016/j.cej.2015.01.066.

Lakayan, S., Behroozsarand, A., Samadi, A., Sirousazar, M., 2020. Electrospun polystyrene/cloisite 20A fiber for selective separation of oil from water surface. J. Environ. Chem. Eng. 103775. https://doi.org/10.1016/j.jece.2020.103775.

Li, H., Wu, W., Bubakir, M.M., Chen, H., Zhong, X., Liu, Z., Ding, Y., Yang, W., 2014. Polypropylene fibers fabricated via a needleless melt-electrospinning device for marine oil-spill cleanup. J. App. Polym. Sci. 131 (7) https://doi.org/10.1002/app.40080.

Mookgo, M., Nthunya, L.N., Gutierrez, L., Matabola, P., Mishra, S., Nxumalo, E.N., 2020. Perfluorooctyltriethoxy silane and carbon nanotubes-modified PVDF superoleophilic nanofibre membrane for oil-in-water adsorption and recovery. J. Environ. Chem. Eng. 8, 104497 https://doi.org/10.1016/j.jece.2020.104497.

Noor, A.-J., Tatjána J. 2016. Review on the effectiveness of adsorbent materials in oil spills clean up. In: *7th International Conference of ICEEE, (pp 131-138)* Budapest, Hungary: 7th ICEEE-2016.

Oribayo, O., Feng, X., Rempel, G.L., Pan, Q., 2017. Synthesis of lignin-based polyurethane/graphene oxide foam and its application as an absorbent for oil spill clean-ups and recovery. J. Chem. Eng. 191–202 https://doi.org/10.1016/j.cej.2017.04.054 1385-8947.

Pablo, G.-S., Hrichi, A., Garrido-Zoido, J.M., Alvarez-Torrellas, S., Marcos Larriba, M., Gil, V., Amor, H.B., García, J., 2024. Natural clays as adsorbents for the efficient removal of antibiotic ciprofloxacin from wastewaters: Experimental and theoretical studies using DFT method. J. Ind. Eng. Chem. 137–151 https://doi.org/10.1016/j.jiec.2023.12.044.

Parmoor, S., Sirousazar, M., Kheiri, F., Kokabi, M., 2020. Polyethylene/clay/graphite nanocomposites as potential materials for preparation of reinforced conductive natural gas transfer pipe, *Iran J. Chem. Eng.* (39) 2, 59–68. 10.30492/IJCCE.2020.33964.

Peigney, A., Laurent, Ch., Flahaut, E., Bacsa, R.R., Rousset, A., 2001. Specific surface area of carbon nanotubes and bundles of carbon nanotubes. J. Carbon 39, 507–514. https://doi.org/10.1016/S0008-6223(00)00155-X.

Pin-Hsuan, C., Min-Chun, S., Pei-Di, J., Ruei-Ci, W., Chen-Bin, W., 2017. Graphene sponge as an efficient and recyclable oil sorbent. *4th Internl Conf. on the Advanct of Materls and Nanotech. (ICAMN IV 2016)* (030005:1 - 10). USA: AIP Publishing. 978-0-7354-1557-7. 10.1063/1.4999861.

Pourjavadi, A., Doulabi, M., Soleyman, R., 2013. Novel carbon-nanotube-based organogels as candidates for oil recovery. J. Polym. Int. 62 (2), 179–183. https://doi.org/10.1002/pi.4274.

Ren, R.P., Li, W., Lv, Y.K., Robust, A., 2017. Superhydrophobic graphene aerogel as a recyclable sorbent for oils and organic solvents at various temperatures. J. Colloid Interface Sci. 1–24 https://doi.org/10.1016/j.jcis.2017.01.071.

Saleem, J., Ning, C., Barford, J., McKay, G., 2015. Combating oil spill problem using plastic waste. J. Waste Manage. 1–5 https://doi.org/10.1016/j.wasman.2015.06.003.

Sandeep, N.T., Srinivasa Rao, G.S., Mathur, A.B., Jasra, R., 2017. Polyolefin/graphene nanocomposites: a review. J. R. Soc. Chem. 7, 23615–23632. https://doi.org/10.1039/C6RA28392F.

Shahriary, L., Athawale, A.A., 2014. Graphene oxide synthesized by using modified hummers approach. Int. J. Renew. Energy Environ. Eng. 02 (01), 58–63.

Timo, S., 1998. Electrical properties of water in clay and silty soils. J. App. Geophys. 40, 73–88. https://doi.org/10.1016/S0926-9851(98)00017-2.

Wang, J., Shi, Z., Jinchen Fan, Yu., Ge, J.Y., Guoxin, Hu., 2012. Self-assembly of graphene into three-dimensional structures promoted by natural phenolic acids. J. Mater. Chem. 22, 22459. https://doi.org/10.1039/C2JM35024F.

Wu, J., An, A.K., Guo, J., Lee, E.J., Farid, M.U., Jeong, S., 2017. CNTs reinforced superhydrophobic-oleophilic electrospun polystyrene oil sorbent for enhanced sorption capacity and reusability. Chem. Eng. J. 314, 526–536. https://doi.org/10.1016/j.cej.2016.12.010.